

Superconductivity in $\text{ThMo}_2\text{Si}_2\text{C}$ with Mo_2C Square Net

Superconductivity in $\text{ThMo}_2\text{Si}_2\text{C}$ with Mo_2C Square Net

Zichen Liu,¹ Baizhuo Li,² Yusen Xiao,¹ Qingchen Duan,¹ Yanwei Cui,³ YuXue Mei¹
 Qian Tao,² Shuli Wei,¹ Shugang Tan,¹ Qiang Jing,¹ Qing Lu,¹ Yuping Sun,¹ Yunyan
 Liu,¹ Shenggui Fu,¹ Hao Jiang,⁴ Zhi Ren,³ Zhu'an Xu,² Cao Wang,^{1*} Guanghan Cao.²

¹*School of Physics and Optoelectronic Engineering,
 Shandong University of Technology, Zibo 255000, P. R. China*

²*Department of Physics, Zhejiang Province Key
 Laboratory of Quantum Technology and Devices,
 Interdisciplinary Center for Quantum Information,
 and State Key Lab of Silicon Materials,
 Zhejiang University, Hangzhou 310027, P. R. China*

³*School of Science, Westlake University,
 18 Shilongshan Road, Hangzhou 310064, P. R. China*

⁴*School of Physics and Optoelectronics,
 Xiangtan University, Xiangtan 411105, P. R. China*

(Dated: April 21, 2021)

Abstract

We report the superconductivity of a new quaternary compound $\text{ThMo}_2\text{Si}_2\text{C}$, synthesized with the arc-melting technique. The compound crystallizes in a tetragonal $\text{CeCr}_2\text{Si}_2\text{C}$ -type structure with cell parameters of $a = 4.2296 \text{ \AA}$ and $c = 5.3571 \text{ \AA}$. An interlayer Si–Si covalent bonding is suggested by the atomic distance. The electrical resistivity and magnetic susceptibility measurements indicate a Pauli-paramagnetic metal with dominant electron–electron scattering in the normal-state. Bulk superconductivity at 2.2 K is demonstrated with a dimensionless specific-heat jump of $\Delta C/\gamma_n T = 0.98$. The superconducting parameters of the critical magnetic fields, coherence length, penetration depth, and superconducting energy gap are given.

* E-mail: wangcao@sdut.edu.cn

I. INTRODUCTION

Since the discovery of high-temperature cuprate superconductors, the exploration of new superconductors has aroused enormous interest in layered compounds, including RNi_2B_2C (R for rare earth),[1] MgB_2 ,[2] Sr_2RuO_4 ,[3] iron pnictides/chalcogenides,[4, 5] and BiS_2 -based compounds.[6] Recently, a new quaternary superconductor $BaTi_2Sb_2O$ has been reported, consisting of alternately stacked Ba planes and Ti_2Sb_2O layers. Upon cooling, the compound undergoes a density-wave-like (DW) transition at 54 K and superconducting transition at 1.2 K.[7–10] The DW ordering can be suppressed by both hole doping in $Ba_{1-x}Na_xTi_2Sb_2O$ and isovalent substitution in $BaTi_2Sb_{2-x}Bi_xO$, where the optimal superconducting T_c s reaches 5.5 K and 3.7 K, respectively.[11, 12] Superconductivity of 4.6 K has also been observed in the undoped end member $BaTi_2Bi_2O$. [13] All these discoveries mark the birth of a new superconducting family based on the Ti_2Pn_2O ($Pn = Sb, Bi$) block layers.[14] If the single-layered Ba atom in the lattice is replaced by fluorite-like Sr_2F_2 or Sm_2O_2 layers, no superconductivity is observed while the DW state prevails.[13, 15] In addition, the coexistence of superconductivity and DW transition was observed in the intergrowth compound $Ba_2Ti_2Fe_2As_4O$, where the superconductivity and the DW instability were ascribed to the Fe_2As_2 and Ti_2As_2O layers, respectively.[16]

The newly discovered superconductors containing Ti_2Pn_2O layers constitute a small fraction of a much larger compound family. Among them, the key structural motif is the anti- CuO_2 -layer-like M_2O square planes, such as Ti_2O , [14] V_2O , [17, 18] Mn_2O , [19] Fe_2O , [20–24] and Co_2O . [25] The M_2O planes are sandwiched by the X (chalcogen, pnictogen) monolayers, forming unique M_2X_2O structural units. We note that a similar M_2X_2O -type structure can also be found in oxygen-free compounds, such as $LaRu_2Al_2B$ and RM_2Si_2C ($M = Cr, Mo$). [26–30] The most distinctive feature of these oxygen-free compounds, compared to oxygen-containing ones, is the $X-X$ interlayer covalent bond, which results in lattice collapse along the c -axis. All these compounds with a collapsed structure show metallic behavior, and the electronic states observed in the vicinity of the Fermi level are mainly dominated by d -orbital electrons. [26, 29, 31] To date, no superconductivity has been reported in these compounds.

Here, we report the synthesis, structure, and physical properties of a new layered carbide $ThMo_2Si_2C$. Powder X-ray diffraction (XRD) indicates that the compound crystallizes in

the $\text{CeCr}_2\text{Si}_2\text{C}$ -type structure with interlayer Si–Si covalent bonds. The compound exhibits metallic behavior with Pauli paramagnetism. Both magnetic susceptibility and electronic resistivity reveal superconductivity of $T_c = 2.2$ K. No charge/spin-density-wave anomaly is observed on the $\chi - T$ and $\rho - T$ curves, which marks the difference to $\text{BaTi}_2\text{Sb}_2\text{O}$. The compound is characterized as a phonon-mediated superconductor with considerable electron–electron interaction.

II. EXPERIMENTAL

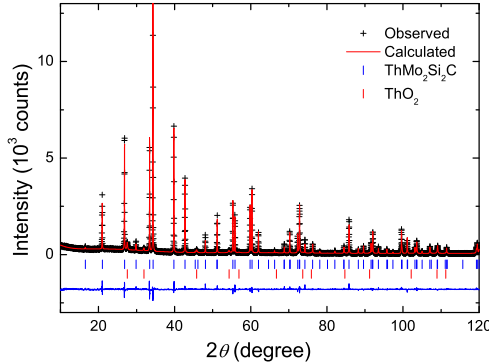


FIG. 1: (Color online) Rietveld refinement profile of $\text{ThMo}_2\text{Si}_2\text{C}$ polycrystalline sample.

A polycrystalline sample of $\text{ThMo}_2\text{Si}_2\text{C}$ was synthesized using powders of Th, Mo (Alfa 99.9%), Si (Alfa 99.99%), and graphite (99.95%) as starting materials. The preparation of thorium metal is described elsewhere.[32] The stoichiometric mixture of the materials were sufficiently mixed in an agate mortar and cold-pressed into a pellet. All these procedures are carried out in a glove box protected by high purity argon. The pellet was then melted by the standard arc-melting technique on a water-cooled copper hearth. The sample was melted five times and was flipped after each melting process to ensure homogeneity. The arc-melted button was placed in an alumina crucible, sealed in an evacuated silica ampoule, and annealed at 1100 °C for two weeks.

Powder XRD was carried out at room temperature on a PANalytical X-ray diffractometer (model EMPYREAN) with monochromatic $\text{Cu K}\alpha_1$ radiation. The crystal structure data were obtained by Rietveld refinement using the step-scan XRD data with $10^\circ \leq 2\theta \leq 120^\circ$, and the diffraction data were refined via the Rietveld method using the program *RIETAN-*

2000.[33] The structural parameters were obtained assuming that the occupancy was the same as the chemical composition. The electrical resistivity was measured in a Quantum Design Physical Property Measurement System (PPMS-9 Dynacool), using a standard four-probe method down to 1.8 K, and then, if necessary, from 1.8 to 0.4 K with an adiabatic dilution refrigerator option. The measurement of specific heat down to 0.4 K with ^3He subassembly was carried out on a Quantum Design PPMS-9 Evercool II using a relaxation method. The dc magnetization measurements down to 0.4 K were performed on a Quantum Design magnetic property measurement system (MPMS3) with a ^3He cryostat.

III. RESULTS AND DISCUSSION

TABLE I: Summary of crystallographic data and refinement parameters for $\text{ThMo}_2\text{Si}_2\text{C}$

Data set	Parameters
space group	$P4/mmm$
a (Å)	4.2296(3)
c (Å)	5.3571(4)
V (Å ³)	95.84(1)
R_{wp} (%)	8.346
S	1.21
Z	1

Figure 1 shows the XRD pattern of $\text{ThMo}_2\text{Si}_2\text{C}$ together with the Rietveld refinement profile for the $\text{CeCr}_2\text{Si}_2\text{C}$ -type structure (space group $P4/mmm$). The obtained lattice parameters for $\text{ThMo}_2\text{Si}_2\text{C}$ are $a = 4.2296(3)$ Å and $c = 5.3571(4)$ Å. A small amount of ThO_2 (3.7 wt.%, according to refinement) is present, which can be ascribed to oxygen contamination during the sample transfer from the glove box to the arc-melting equipment. Table I lists the refined crystal structure parameters. Table II shows the coordinates and temperature factors for all the atoms in the lattice. Figure 2 shows the crystal lattice of $\text{ThMo}_2\text{Si}_2\text{C}$ and the details of the $\text{Mo}_2\text{Si}_2\text{C}$ block layer. Table III compares the lattice parameters of $\text{ThMo}_2\text{Si}_2\text{C}$ with those of the isostructural compounds $\text{CeMo}_2\text{Si}_2\text{C}$ and $\text{PrMo}_2\text{Si}_2\text{C}$. According to the refinement, the interlayer's nearest Si-Si distance ($d_{\text{Si-Si}}$) is 2.429 Å. This Si-Si distance is similar to that of silicon with a diamond-type structure (2.352

Å), and thus should be considered a single Si–Si bond. Therefore, the structure of $\text{ThMo}_2\text{Si}_2\text{C}$ is of the $\text{CeCr}_2\text{Si}_2\text{C}$ -type collapsed phase. As is well known, the ionic radius of Th^{4+} (0.94 Å, $CN = 6$) is smaller than that of Pr^{3+} (0.99 Å) or Ce^{3+} (1.01 Å).[34] However, we note that the cell volume does not follow the radius trend of the rare-earth elements. Moreover, the a -axis of $\text{ThMo}_2\text{Si}_2\text{C}$ is the longest among the three compounds. This can be understood as an electron-doping effect, as Th^{4+} contributes more electrons than Pr^{3+} or Ce^{3+} . On the one hand, the electron transferred to the Mo_2C plane expands the a -axis by elongating the Mo–C bond. On the other hand, the charge transfer strengthens the interlayer Coulomb attraction and results in the shrinkage of the c -axis. We note that similar phenomena are quite common in iron arsenide superconductors, where electron doping can cause a decrease in axial ratio c/a . [35, 36]

TABLE II: Atomic coordinates and temperature factors for all the elements in $\text{ThMo}_2\text{Si}_2\text{C}$

atom	site	x	y	z	B
Th	1a	0	0	0	0.1(fixed)
Mo	2e	0	1/2	1/2	0.15(3)
Si	2h	1/2	1/2	0.2267(6)	0.17(7)
C	1b	0	0	1/2	1.9(5)

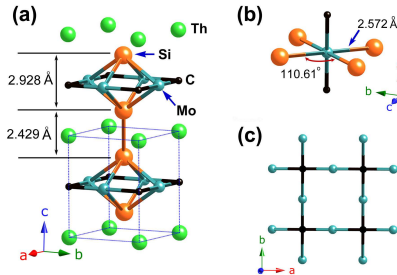


FIG. 2: (Color online) (a) Crystal structure of $\text{ThMo}_2\text{Si}_2\text{C}$. (b) Schematic of the distorted MoSi_4C_2 octahedron. (c) Bird's-eye view of the Mo_2C square lattice.

Figure 3 shows the resistivity data of the $\text{ThMo}_2\text{Si}_2\text{C}$ sample. The zero-field resistivity at 300 K is 1.19 $\text{m}\Omega\cdot\text{cm}$, which is similar to that of $\text{CeMo}_2\text{Si}_2\text{C}$. [29] Upon cooling, the resistivity exhibits metallic behavior without anomaly. A superconducting transition is revealed by an abrupt resistivity drop at 2.2 K. The residual resistivity is high, suggesting that the sample

TABLE III: Lattice parameters of $R\text{Mo}_2\text{Si}_2\text{C}$ ($R = \text{Ce}, \text{Pr}, \text{Th}$), where h_{Si} and $d_{\text{Si-Si}}$ represent the vertical distance from Si to the Mo_2C plane and the interlayer Si-Si distance.

Compound	a -axis (Å)	c -axis (Å)	c/a	V_{cell} (Å ³)	h_{Si} (Å)	$d_{\text{Si-Si}}$ (Å)
CeMo ₂ Si ₂ C[29]	4.213	5.376	1.276	95.42	1.512	2.353
PrMo ₂ Si ₂ C[30]	4.2139	5.4093	1.284	96.05	1.508	2.393
ThMo ₂ Si ₂ C	4.2296	5.3571	1.267	95.84	1.464	2.429

may be in the dirty limit. The normal-state resistivity below 40 K can be fitted using the equation

$$\rho(T) = \rho_0 + AT^2 + \alpha \left(\frac{T}{\Theta_R} \right)^n \int_0^{\Theta_R/T} \frac{x^n}{(e^x - 1)(1 - e^{-x})} dx \quad (1)$$

where Θ_R is the Debye temperature obtained from the resistivity measurements and matches very closely with that obtained from the specific heat. The best fit appears while the constant n in the last term of the equation (contribution of electron-phonon scattering) is 2. The fitting parameters are $\rho_0 = 0.35 \text{ m}\Omega\cdot\text{cm}$ and $A = 2.75 \times 10^{-5} \text{ m}\Omega\cdot\text{cm}\cdot\text{K}^{-2}$. Figure 3(b) shows the temperature dependence of resistivity under static magnetic fields (0 T, 0.05 T, 0.1 T, 0.15 T, 0.2 T, 0.25 T). We define $T_c(H)$ as the temperature where the resistivity falls to 90% of the normal-state value. As shown in Figure 3(c), the temperature dependence of the upper critical field (H_{c2}) increases approximately linearly upon cooling to the lowest temperature measured. Thus, the upper critical field at 0 K is estimated from linear extrapolation to be $H_{c2}(0) = 2660 \text{ Oe}$, and the coherent length can be calculated as $\xi = 352 \text{ \AA}$ according to the relation $\mu_0 H_{c2}(0) = \Phi_0/2\pi\xi^2$, where Φ_0 is the magnetic flux quantum.

Figure 4(a) plots the temperature dependence of magnetic susceptibility at $H = 10 \text{ Oe}$. Both zero-field-cooling (ZFC) and field-cooling (FC) protocols are employed in the measurement. A strong diamagnetic signal below 2.2 K confirms the superconducting transition observed in the resistivity measurement. The magnetic shielding fraction at 0.4 K exceeds 100% due to the demagnetization effect, indicating bulk superconductivity. The shoulder-like susceptibility (ZFC) around 1.5 K is probably due to the intergrain weak-link effect. The susceptibility measured at $H = 10^4 \text{ Oe}$ is shown in Figure 4(b). The room temperature susceptibility is $1.38 \times 10^{-4} \text{ emu}\cdot\text{mol}^{-1}$. The susceptibility increases gradually upon cooling. We fit the susceptibility data using the extended Curie-Weiss law $\chi = \chi_0 + C/(T - \theta)$ over a temperature region of $10 \text{ K} \leq T \leq 300 \text{ K}$. The derived

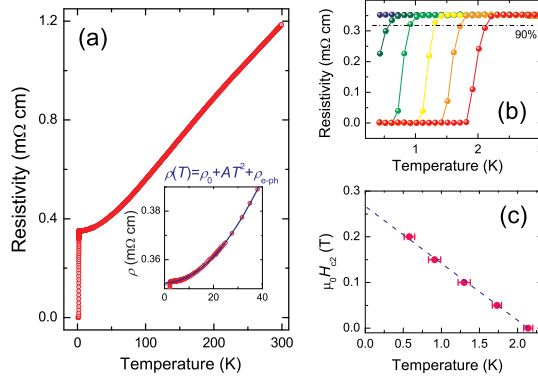


FIG. 3: (Color online) (a) Temperature dependence of resistivity at zero magnetic field for the $\text{ThMo}_2\text{Si}_2\text{C}$ polycrystalline sample. The inset shows the normal-state resistivity below 40 K. The blue line fits the data using the equation $\rho(T) = \rho_0 + AT^2 + \rho_{e\text{-ph}}$, where $\rho_{e\text{-ph}}$ represents the contribution of electron–phonon scattering. (b) Temperature dependence of resistivity near the superconducting transition measured in selected magnetic fields. (c) Temperature dependence of the upper critical field.

parameters are $\chi_0 = 1.3 \times 10^{-4} \text{ emu}\cdot\text{mol}^{-1}$, $C = 2.01 \times 10^{-3} \text{ emu}\cdot\text{K}\cdot\text{mol}^{-1}$, and $\theta = -1.9 \text{ K}$. The results suggest that $\text{ThMo}_2\text{Si}_2\text{C}$ is a metal with Pauli paramagnetism. The Curie constant corresponds to a tiny effective magnetic moment of $0.12 \mu_B/\text{f.u.}$, which may be due to a small amount of paramagnetic impurities.

Figure 5 shows the field dependence of the zero-field cooled magnetization at various temperatures for $\text{ThMo}_2\text{Si}_2\text{C}$. The lower critical field H_{c1} is plotted as a function of $(T/T_c)^2$. We fit the data using the Ginzburg–Landau theory $H_{c1}(T) = H_{c1}(0)[1 - (T/T_c)^2]$ (where $T_c = 2.2 \text{ K}$) and obtain the lower critical field $H_{c1}(0) = 16 \text{ Oe}$. Then the penetration depth and the Ginzburg–Landau parameter are derived as $\lambda = 5280 \text{ \AA}$ and $\kappa = 15$ from the relation $\mu_0 H_{c1}(0) = \ln(\lambda/\xi)\Phi_0/(4\pi\lambda^2)$ and $\kappa = \lambda/\xi$, respectively. Also, the thermodynamic critical field at zero temperature $H_c(0)$ is estimated as 183 Oe .

Figure 6 shows the temperature dependence of the specific heat measured under zero magnetic field. To make the specific heat of normal-state more intuitive, we plot C/T as a function of T^2 from 5 K down to 0.4 K. The data show good linear T^2 dependence of C/T above superconducting T_c , indicating that the specific heat comprises two contributions: the electronic part, which is proportional to T , and the phonon part, which is proportional to T^3 at low temperatures. We fit the specific heat of the normal-state below 5 K using the

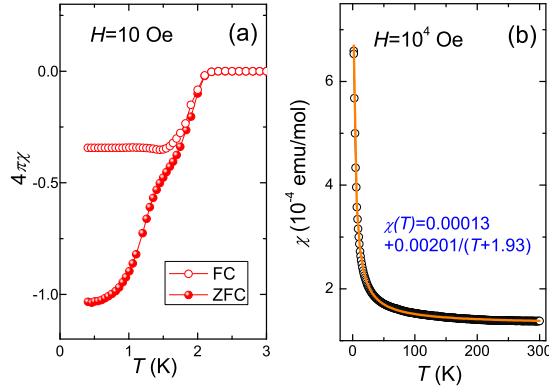


FIG. 4: (Color online) (a) Temperature dependence of magnetic susceptibility measured at $H = 10$ Oe for $\text{ThMo}_2\text{Si}_2\text{C}$. (b) Magnetic susceptibility measured at $H = 10^4$ Oe. The orange solid line fits the normal-state $\chi - T$ curve using the equation $\chi(T) = \chi_0 + C/(T - \theta)$.

relation $C = \gamma_n T + \beta T^3$. The parameters of the electron and phonon are determined as $\gamma_n = 11.4 \text{ mJ}\cdot\text{mol}^{-1}\cdot\text{K}^{-2}$ and $\beta = 2.7 \text{ mJ}\cdot\text{mol}^{-1}\cdot\text{K}^{-4}$ respectively. According to the formula $\Theta_D = [12\pi^4 NR/(5\beta)]^{1/3}$, the Debye temperature Θ_D is estimated to be 351 K.

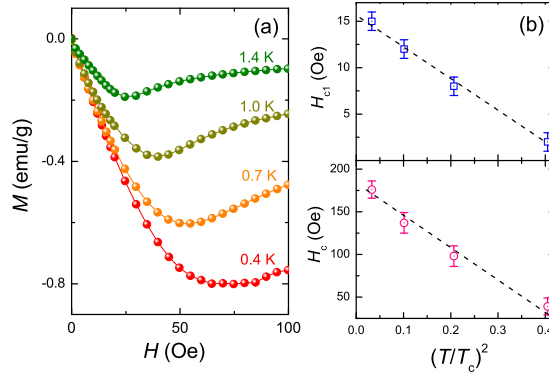


FIG. 5: (Color online) (a) Field dependence of magnetization for $\text{ThMo}_2\text{Si}_2\text{C}$ at various temperatures. (b) The lower critical field H_{c1} and the thermodynamic critical field H_c for $\text{ThMo}_2\text{Si}_2\text{C}$ as a function of $(T/T_c)^2$.

Below the T_c , a distinct peak in specific heat is observed. We subtract the normal-state specific heat using the aforementioned fitted data $C = \gamma_n T + \beta T^3$. The inset of Figure 6 plots $\Delta C/\gamma_n T$ versus T/T_c^{th} , where $T_c^{\text{th}} = 2$ K denotes the thermodynamic critical temperature considering entropy conservation. Supposing that an isotropic single-gap model can be adopted here, we fit the specific heat below 1.6 K with the exponential law $C_e \sim$

$\exp(-\Delta_0/k_B T)$. The derived energy gap is $\Delta_0^{\text{exp}} = 0.29$ meV, which matches the Bardeen–Cooper–Schrieffer (BCS) value of 0.30 meV based on the relation $\Delta_0^{\text{BCS}} = 1.76k_B T_c^{\text{th}}$. Further, the electronic specific heat jump at T_c^{th} brings $\Delta C/\gamma_n T = 0.98$, which is smaller than the BCS value of $\Delta C/\gamma_n T = 1.43$. A possible explanation for this deviation is the presence of nonsuperconducting impurities (e.g., ThO₂) and/or amorphous grain-boundary that does not contribute to the signal of superconducting transition. Assuming that the electron–phonon coupling dominates the origin of the superconductivity in ThMo₂Si₂C, the coupling strength λ_{ph} can be estimated from the McMillan formula

$$\lambda_{\text{ph}} = \frac{1.04 + \mu^* \ln\left(\frac{\Theta_D}{1.45T_c}\right)}{(1 - 0.62\mu^*) \ln\left(\frac{\Theta_D}{1.45T_c}\right) - 1.04} \quad (2)$$

where $\mu^* = 0.13$ is the Coulomb pseudopotential for polyvalent transition metals.[37] Using this formula, λ_{ph} was evaluated to be 0.49, suggesting that the superconductivity in ThMo₂Si₂C is in the weak or intermediate coupling regime.

The Wilson ratio (R_W) that reflects the electron–electron correlations in a material can be calculated using the formula $R_W = \chi_P/(3\gamma_n) \times (\pi k_B/\mu_B)^2$, where χ_P represents the Pauli paramagnetic susceptibility.[38] During the Curie-Weiss fitting of the magnetic susceptibility, we get the temperature independent susceptibility $\chi_0 = 1.3 \times 10^{-4}$ emu·mol⁻¹. Note that the fitted χ_0 includes the orbital diamagnetism contribution due to ion cores χ_{core} . If the nominal valences can be represented by the formula Th⁴⁺Mo₂³⁺Si₂³⁻C⁴⁻, then the diamagnetic contribution for ThMo₂Si₂C can be estimated as $\chi_{\text{core}} = -1.01 \times 10^{-4}$ emu·mol⁻¹ using the data listed by G. A. Bain and J. F. Berry.[39] Thus the Pauli-paramagnetic contribution reaches $\chi_P = 2.3 \times 10^{-4}$ emu·mol⁻¹. Then, the Wilson ratio is determined as $R_W = 1.48$, which should be close to 1 in a noninteracting Fermi-liquid system. This indicates that the compound contains considerable electron–electron interaction.

Another important parameter characterizing Fermi-liquid properties is the Kadowaki–Woods ratio ($R_{\text{KW}} = A/\gamma^2$), which presents the relationship between the electron–electron scattering rate and the electron-mass renormalization.[40–43] This ratio is found to be approximately constant within a certain class of materials. For transition metals and heavy-fermion compounds, R_{KW} s are typically 0.4 and 10 $\mu\Omega\cdot\text{cm}\cdot\text{mol}^2\cdot\text{K}^2\cdot\text{J}^{-2}$, respectively. Interestingly, our results provide a much larger $R_{\text{KW}} = 212 \mu\Omega\cdot\text{cm}\cdot\text{mol}^2\cdot\text{K}^2\cdot\text{J}^{-2}$ for ThMo₂Si₂C. Note that R_{KW} is sometime material-dependent and sensitive to dimensionality, electron density, multiband effect, and the interlayer hopping integral.[42–44] To our knowledge,

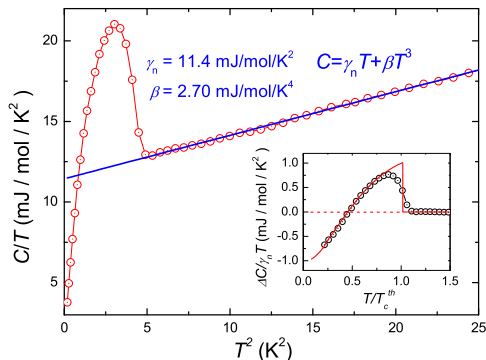


FIG. 6: (Color online) The specific heat coefficient C/T of $\text{ThMo}_2\text{Si}_2\text{C}$ as a function of T^2 . The inset plots the normalized electronic specific heat $\Delta C/\gamma_n T$ after subtracting the normal-state contribution. The solid red line presents the fit with the conventional BCS model.

large R_{KW} values are usually observed in strongly correlated transition-metal oxides or organic superconductors, such as $\text{La}_{1.7}\text{Sr}_{0.3}\text{CuO}_4$ ($52 \mu\Omega\cdot\text{cm}\cdot\text{mol}^2\cdot\text{K}^2\cdot\text{J}^{-2}$), $\text{Na}_{0.7}\text{CoO}_2$ ($600 \mu\Omega\cdot\text{cm}\cdot\text{mol}^2\cdot\text{K}^2\cdot\text{J}^{-2}$), and $\beta\text{-ET}_2\text{I}_3$ ($347 \mu\Omega\cdot\text{cm}\cdot\text{mol}^2\cdot\text{K}^2\cdot\text{J}^{-2}$).^[42, 44–47] Aside from the intrinsic mechanism for large R_{KWS} , we note that the magnetic impurities in a polycrystalline sample may affect the fitting parameter A in the $\rho(T)$ equation, which in turn can lead to overestimation of R_{KW} . Thus, high-quality samples, preferably single crystals, are needed to clarify this issue.

Now let us discuss the electronic states in the $\text{CeCr}_2\text{Si}_2\text{C}$ -type family. So far, superconductivity has only been observed in members containing Ti_2O or Mo_2C planes. For Ti_2O -based compounds, superconductivity competes with the DW ordering state, which is ascribed to Fermi-surface nesting or p - d orbital ordering.^[10, 48] For compounds containing Mo_2C -plane, the DW ordering is absent. We note that the DW state is also absent among the members containing Cr_2C -plane. This suggests the origin of superconductivity in the carbides is different from that in the Ti_2O -based compounds. Very recently, neutron diffraction works on the nonsuperconductive compound $\text{UCr}_2\text{Si}_2\text{C}$ identified an antiferromagnetic ordering of Cr magnetic moment ($\sim 0.6 \mu_{\text{B}}$) at 300 K.^[49] However, similar experiments on the isostructural compounds $\text{LnCr}_2\text{Si}_2\text{C}$ (Ln for lanthanides) did not recognize any Cr moment.^[31] For the compounds based on $\text{Mo}_2\text{Si}_2\text{C}$ layers, superconductivity was only observed in $\text{ThMo}_2\text{Si}_2\text{C}$ rather than $\text{LnMo}_2\text{Si}_2\text{C}$.^[29, 30] Considering the different nominal valence of $(\text{U}/\text{Th})^{4+}$ and Ln^{3+} , one may conclude that the electron configuration plays a crucial role in determining

the d -orbital states in Cr_2C and Mo_2C planes. As the chemical valence of Cr/Mo is also affected by the interlayer Si-Si bond order, which is sensitive to the Si-Si bond length, additional theoretical and experimental works are needed to determine the configuration of the d -orbital in the materials.

IV. CONCLUDING REMARKS

We have synthesized a new quaternary compound $\text{ThMo}_2\text{Si}_2\text{C}$ with superconducting $T_c = 2.2$ K. This is the first superconductor among the $\text{CeCr}_2\text{Si}_2\text{C}$ -type carbides. The lower, upper, and thermodynamic critical fields at zero temperature are determined to be $H_{c1} = 16$ Oe, $H_{c2} = 2660$ Oe and $H_c = 183$ Oe, respectively. Then, the penetration depth, coherent length, and Ginzburg-Landau parameter are calculated accordingly as $\lambda = 5280$ Å, $\xi = 352$ Å, and $\kappa = 15$. Although the jump of specific heat due to the superconducting transition deviates from that predicted by the BCS theory, the superconducting energy gap derived by fitting the specific heat below the T_c precisely matches the theoretical value. The Wilson ratio and Kadowaki-Woods ratio are obtained as $R_W = 1.48$ and $R_{KW} = 212$. Our data indicate that $\text{ThMo}_2\text{Si}_2\text{C}$ is a BCS superconductor with considerable electron-electron interaction. More efforts should be made to explore new superconductors among compounds with similar crystal structures.

Acknowledgments

This work was supported by the National Key Research and Development Program of China (Grant No. 2017YFA0303002) and the Natural Science Foundation of Shandong Province (Grants No. ZR2019MA036 and ZR2016AQ08).

-
- [1] R. J. Cava, H. Takagi, H. W. Zandbergen, J. J. Krajewski, W. F. Peck Jr, T. Siegrist, B. Batlogg, R. B. van Dover, R. J. Felder, K. Mizuhashi, J. O. Lee, H. Eisaki, and S. Uchida, *Nature* **367**, 252 (1994).
 - [2] J. Nagamatsu, N. Nakagawa, T. Muranaka, Y. Zenitani, and J. Akimitsu, *Nature* **410**, 63 (2001).

- [3] Y. Maeno, H. Hashimoto, K. Yoshida, S. Nishizaki, T. Fujita, J. G. Bednorz, and F. Lichtenberg, *Nature* **372**, 532 (1994).
- [4] Y. Kamihara, T. Watanabe, M. Hirano, and H. Hosono, *J. Am. Chem. Soc.* **130**, 3296 (2008).
- [5] F. Hsu, J. Luo, K. Yeh, T. Chen, T. Huang, P. M. Wu, Y. Lee, Y. Huang, Y. Chu, D. Yan, and M. Wu, *PNAS* **105**, 14262 (2008).
- [6] Y. Mizuguchi, S. Demura, K. Deguchi, Y. Takano, H. Fujihisa, Y. Gotoh, H. Izawa, and O. Miura, *J. Phys. Soc. Jpn.* **81**, 114725 (2012).
- [7] T. Yajima, K. Nakano, F. Takeiri, T. Ono, Y. Hosokoshi, Y. Matsushita, J. Hester, Y. Kobayashi, and H. Kageyama, *J. Phys. Soc. Jpn.* **81**, 103706 (2012).
- [8] S. Kitagawa, K. Ishida, K. Nakano, T. Yajima, and H. Kageyama, *Phys. Rev. B* **87**, 060510(R) (2013).
- [9] Y. Nozaki, K. Nakano, T. Yajima, H. Kageyama, B. Frandsen, L. Liu, S. Cheung, T. Goko, Y. J. Uemura, T. S. J. Munsie, T. Medina, G. M. Luke, J. Munevar, D. Nishio-Hamane, and C. M. Brown, *Phys. Rev. B* **88**, 214506 (2013).
- [10] Q. Song, Y. J. Yan, Z. R. Ye, M. Q. Ren, D. F. Xu, S. Y. Tan, X. H. Niu, B. P. Xie, T. Zhang, R. Peng, H. C. Xu, J. Jiang, and D. L. Feng, *Phys. Rev. B* **93**, 024508 (2016).
- [11] P. Doan, M. Gooch, Z. Tang, B. Lorenz, A. Möller, J. Tapp, P. C. W. Chu, and A. M. Guloy, *J. Am. Chem. Soc.* **134**, 16520 (2012).
- [12] H. F. Zhai, W. H. Jiao, Y. L. Sun, J. K. Bao, H. Jiang, X. J. Yang, Z. T. Tang, Q. Tao, X. F. Xu, Y. K. Li, C. Cao, J. H. Dai, Z. A. Xu, and G. H. Cao, *Phys. Rev. B* **87**, 100502(R) (2013).
- [13] T. Yajima, K. Nakano, F. Takeiri, J. Hester, T. Yamamoto, Y. Kobayashi, N. Tsuji, J. Kim, A. Fujiwara, and H. Kageyama, *J. Phys. Soc. Jpn.* **82**, 013703 (2013).
- [14] T. Yajima, *Condens. Matter* **2**, 4 (2017).
- [15] R. H. Liu, Y. A. Song, Q. J. Li, J. J. Ying, Y. J. Yan, Y. He, and X. H. Chen, *Chem. Mater.* **22**, 1503 (2010).
- [16] Y. L. Sun, H. Jiang, H. F. Zhai, J. K. Bao, W. H. Jiao, Q. Tao, C. Y. Shen, Y. W. Zeng, Z. A. Xu, and G. H. Cao, *J. Am. Chem. Soc.* **134**, 12893 (2012).
- [17] M. Valldor, P. Merz, Y. Prots, and W. Schnelle, *Eur. J. Inorg. Chem.* **2016**, 23.
- [18] A. Ablimit, Y. L. Sun, H. Jiang, S. Q. Wu, Y. B. Liu, and G. H. Cao, *Phys. Rev. B* **97**, 214517 (2018).

- [19] N. Ni, E. Climent-Pascual, S. Jia, Q. Huang, and R. J. Cava, *Phys. Rev. B* **82**, 214419 (2010).
- [20] J. M. Mayer, L. F. Schneemeyer, T. Siegrist, J. V. Waszczak, and B. Van Dover, *Angew. Chem. Int. Ed. Engl.* **31**, 1645 (1992).
- [21] H. Kabbour, E. Janod, B. Corraze, M. Danot, C. Lee, M. H. Whangbo, and L. Cario, *J. Am. Chem. Soc.* **130**, 8261 (2008).
- [22] J. B. He, D. M. Wang, H. L. Shi, H. X. Yang, J. Q. Li, and G. F. Chen, *Phys. Rev. B* **84**, 205212 (2011).
- [23] F. Takeiri, Y. Matsumoto, T. Yamamoto, N. Hayashi, Z. Li, T. Tohyama, C. Tassel, C. Ritter, Y. Narumi, M. Hagiwara, and H. Kageyama, *Phys. Rev. B* **94**, 184426 (2016).
- [24] H. Zhang, X. Wu, D. Li, S. Jin, X. Chen, T. Zhang, Z. Lin, S. Shen, D. Yuan, and X. Chen, *J. Phys.: Condens. Matt.* **28**, 145701 (2016).
- [25] C. Wang, M. Q. Tan, C. M. Feng, Z. F. Ma, S. Jiang, Z. A. Xu, G. H. Cao, K. Matsubayashi, and Y. Uwatoko, *J. Am. Chem. Soc.* **132**, 7069 (2010).
- [26] J. V. Zaikina, Y. Jo, and S. E. Latturmer, *Inorg. Chem.* **49**, 2773 (2010).
- [27] C. Tang, S. Fan, M. Zhu, *J. Alloys Compd.* **299**, 1 (2000).
- [28] M. W. Pohlkamp, and W. Jeitschko, *Z. Naturforsch.* **56b**, 1143 (2001).
- [29] U. B. Paramanik, Anupam, U. Burkhardt, R. Prasad, C. Geibel, and Z. Hossain, *J. Alloys Compd.* **580**, 435 (2013).
- [30] E. Dashjav, W. Schnelle, F. R. Wagner, G. Kreiner, and R. Kniep, *Z. Kristallogr. NCS* **221**, 267 (2006).
- [31] V. Klosek, A. Vernière, B. Malaman, J. Tobola, and S. Kaprzyk, *Phys. Rev. B* **78**, 104419 (2008).
- [32] C. Wang, Z. C. Wang, Y. X. Mei, Y. K. Li, L. Li, Z. T. Tang, Y. Liu, P. Zhang, H. F. Zhai, Z. A. Xu, and G. H. Cao, *J. Am. Chem. Soc.* **138**, 2170 (2016).
- [33] F. Izumi, and T. Ikeda, *Mater. Sci. Forum.* **198**, 321 (2000).
- [34] J. A. Dean, *Lange's Handbook of Chemistry*, 15th ed. (McGraw-Hill Education: New York, 1998).
- [35] C. Wang, L. J. Li, S. Chi, Z. W. Zhu, Z. Ren, Y. K. Li, Y. T. Wang, X. Lin, Y. K. Luo, S. Jiang, X. F. Xu, G. H. Cao, and Z. A. Xu, *Europhys. Lett.* **83**, 67006 (2008).
- [36] C. Wang, Y. K. Li, Z. W. Zhu, S. Jiang, X. Lin, Y. K. Luo, S. Chi, L. J. Li, Z. Ren, M. He, H. Chen, Y. T. Wang, Q. Tao, G. H. Cao, and Z. A. Xu, *Phys. Rev. B* **79**, 054521 (2009).

- [37] W. L. McMillan, *Phys. Rev.* **167**, 331 (1968).
- [38] G. R. Stewart, *Rev. Mod. Phys.* **56**, 755 (1984).
- [39] G. A. Bain, and J. F. Berry, *J. Chem. Educ.* **85**, 532 (2008).
- [40] M. J. Rice, *Phys. Rev. Lett.* **20**, 1439 (1968).
- [41] K. Kadowaki, and S. B. Woods, *Solid State Commun.* **58**, 507 (1986).
- [42] N. E. Hussey, *J. Phys. Soc. Jpn.* **74**, 1107 (2005).
- [43] A. C. Jacko, J. O. Fjærestad, and B. J. Powell, *Nat. Phys.* **5**, 422 (2009).
- [44] S. Y. Li, L. Taillefer, D. G. Hawthorn, M. A. Tanatar, J. Paglione, M. Sutherland, R. W. Hill, C. H. Wang, and X. H. Chen, *Phys. Rev. Lett.* **93**, 056401 (2004).
- [45] S. Nakamae, K. Behnia, N. Mangkorntong, M. Nohara, H. Takagi, S. J. C. Yates, and N. E. Hussey, *Phys. Rev. B* **68**, 100502(R) (2003).
- [46] G. R. Stewart, J. O'Rourke, G. W. Crabtree, K. D. Carlson, H. H. Wang, J. M. Williams, F. Gross, and K. Andres, *Phys. Rev. B* **33**, 2046(R) (1986).
- [47] L. N. Bulaevskii, *Adv. Phys.* **37**, 443 (1988).
- [48] D. W. Song, J. Li, D. Zhao, L. K. Ma, L. X. Zheng, S. J. Li, L. P. Nie, X. G. Luo, Z. P. Yin, T. Wu, and X. H. Chen, *Phys. Rev. B* **98**, 235142 (2018).
- [49] P. Lemoine, A. Vernière, M. Pasturel, G. Venturini, and B. Malaman, *Inorg. Chem.* **57**, 2546 (2018).